

University of Groningen

## A Universal Nanogel-Based Coating Approach for Medical Implant Materials

Ghosh, Devlina; Keskin, Damla; Forson, Abigail; Rosman, C.W.K; Bron, Reinier; Siebenmorgen, Clío; Zu, Guangyue; Lasorsa, Alessia; van der Wel, Patrick; van Kooten, Theo G

*Published in:*  
Advanced NanoBiomed Research

*DOI:*  
[10.1002/anbr.202200141](https://doi.org/10.1002/anbr.202200141)

**IMPORTANT NOTE:** You are advised to consult the publisher's version (publisher's PDF) if you wish to cite from it. Please check the document version below.

*Document Version*  
Publisher's PDF, also known as Version of record

*Publication date:*  
2023

[Link to publication in University of Groningen/UMCG research database](#)

*Citation for published version (APA):*

Ghosh, D., Keskin, D., Forson, A., Rosman, C. W. K., Bron, R., Siebenmorgen, C., Zu, G., Lasorsa, A., van der Wel, P., van Kooten, T. G., Witjes, M., Sjollema, J., van der Mei, H. C., & van Rijn, P. (2023). A Universal Nanogel-Based Coating Approach for Medical Implant Materials. *Advanced NanoBiomed Research*, 3(7), Article 2200141. <https://doi.org/10.1002/anbr.202200141>

### Copyright

Other than for strictly personal use, it is not permitted to download or to forward/distribute the text or part of it without the consent of the author(s) and/or copyright holder(s), unless the work is under an open content license (like Creative Commons).

The publication may also be distributed here under the terms of Article 25fa of the Dutch Copyright Act, indicated by the "Taverne" license. More information can be found on the University of Groningen website: <https://www.rug.nl/library/open-access/self-archiving-pure/taverne-amendment>.

### Take-down policy

If you believe that this document breaches copyright please contact us providing details, and we will remove access to the work immediately and investigate your claim.

Downloaded from the University of Groningen/UMCG research database (Pure): <http://www.rug.nl/research/portal>. For technical reasons the number of authors shown on this cover page is limited to 10 maximum.

# A Universal Nanogel-Based Coating Approach for Medical Implant Materials

Devlina Ghosh, Damla Keskin, Abigail M. Forson, Colin W. K. Rosman, Reinier Bron, Clio M. Siebenmorgen, Guangyue Zu, Alessia Lasorsa, Patrick C. A. Van Der Wel, Theo G. Van Kooten, Max J. H. Witjes, Jelmer Sjollema, Henny C. Van Der Mei, and Patrick Van Rijn\*

Coatings are essential for biomedical applications antifouling and antimicrobial properties, supporting cell adhesion and tissue integration and particularly interesting in this field are nanogel (nGel)-based coatings. Since biomaterials differ in physicochemical properties, specific nGel-coating strategies need to be developed for every distinct material, leading to complex coating strategies. Hence, the solution lies in adopting a universal strategy to apply the same nGel coating with the same function on a wide range of implant surfaces. To this end, a universal nGel-based coating approach provides the same coating using a single method on implant materials including stiff polymer materials, metals, ceramics, glass, and elastomers. The coating formation is achieved by electrostatic interactions between oxygen plasma-activated surfaces and positively charged nGels using a spray-deposition method. Fluorescent labels are introduced into the nGels as a model for post-modification capabilities to increase the functionality of the coating. The coating is highly stable under in vitro physiological conditions with the retention of its function on different clinically relevant materials. Meanwhile, the in vivo study indicates that the nGel coating on a polyvinylidene fluoride hernia mesh is stable and biocompatible, therefore, making the coating and the coating strategy, a highly impactful approach for future clinical developments.

## 1. Introduction

Materials for biomedical applications have revolutionized healthcare and provide tremendous support for patients as the materials enable improved monitoring technology,<sup>[1,2]</sup> enhanced drug delivery at targeted sites,<sup>[3,4]</sup> or restoring tissue and organ functions.<sup>[2,5]</sup> Although biomaterials (implants) offer much support and treatments for medical conditions, they can still fail due to secondary complications such as infection and inflammation due to microbial growth and biofilm formation,<sup>[6,7]</sup> immune response in the host body,<sup>[8]</sup> poor tissue integration,<sup>[9]</sup> or any possible preexisting medical history of the patient.<sup>[10]</sup> The aforementioned aspects decide the success or failure of the implant inside the human body.<sup>[11]</sup>


Coatings have been regarded as an excellent possibility to induce desired responses or prevent complications as the bulk implant material does not need to be altered.<sup>[12]</sup> A previously developed coating, based on nanogels (nGels), offers great possibilities as a coating for being antifouling toward proteins, bacteria, and mammalian cells as well as the possibility of providing controlled release strategies.<sup>[13]</sup> A nGel is a highly cross-linked nanometer-sized hydrogel particle<sup>[14,15]</sup> that has been used in many

and mammalian cells as well as the possibility of providing controlled release strategies.<sup>[13]</sup> A nGel is a highly cross-linked nanometer-sized hydrogel particle<sup>[14,15]</sup> that has been used in many

D. Ghosh, D. Keskin, A. M. Forson, C. W. K. Rosman, R. Bron, C. M. Siebenmorgen, G. Zu, T. G. Van Kooten, J. Sjollema, H. C. Van Der Mei, P. Van Rijn  
Department of Biomedical Engineering-FB40  
University of Groningen  
University Medical Center Groningen  
Antonius Deusinglaan 1, 9713 AV Groningen, The Netherlands  
E-mail: p.van.rijn@umcg.nl

A. Lasorsa, P. C. A. Van Der Wel  
Zernike Institute for Advanced Materials  
University of Groningen  
Nijenborgh 4, 9747 AG Groningen, The Netherlands

M. J. H. Witjes  
Department of Oral and Maxillofacial Surgery  
University of Groningen  
University Medical Center Groningen  
Hanzeplein 1 BB70, 9713 GX Groningen, The Netherlands

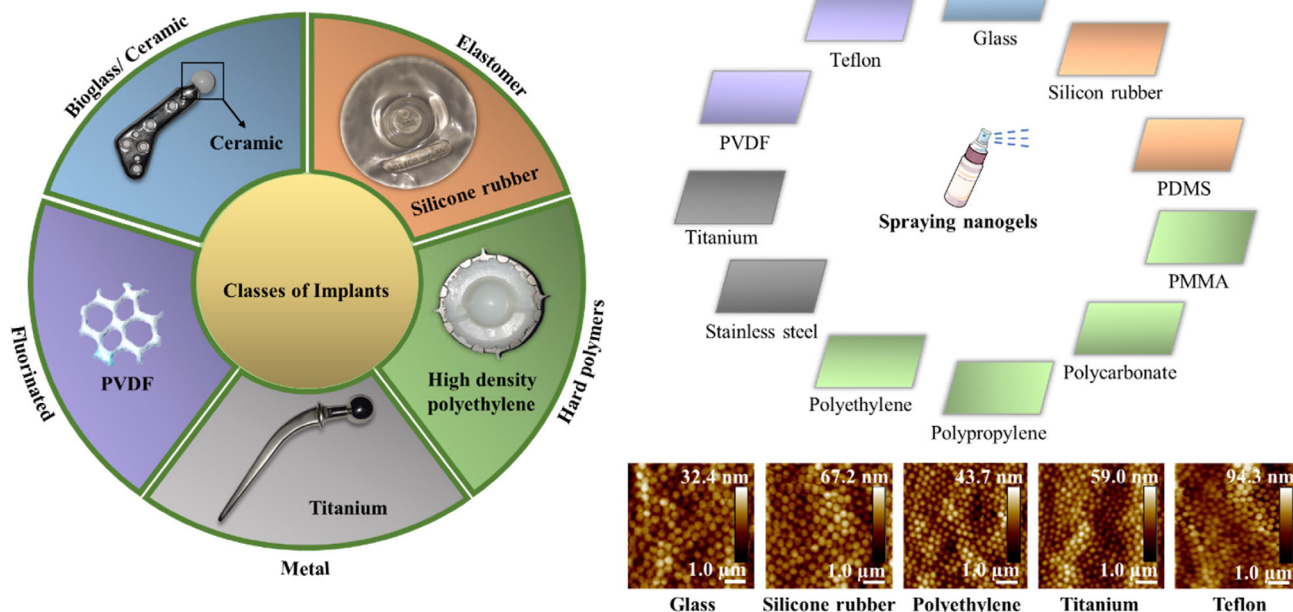
 The ORCID identification number(s) for the author(s) of this article can be found under <https://doi.org/10.1002/anbr.202200141>.

© 2023 The Authors. Advanced NanoBiomed Research published by Wiley-VCH GmbH. This is an open access article under the terms of the Creative Commons Attribution License, which permits use, distribution and reproduction in any medium, provided the original work is properly cited.

DOI: 10.1002/anbr.202200141

systems as responsive nanomaterial due to the possibility of incorporating thermoresponsive properties,<sup>[16–18]</sup> but also responding toward pH,<sup>[19]</sup> light,<sup>[20]</sup> or redox chemistry.<sup>[21]</sup> Additionally, due to the hydrogel properties these particles are also of interest as carriers for delivery<sup>[22–25]</sup> of drugs or other biological molecules and proteins<sup>[25]</sup> that may be applied in regenerative medicine,<sup>[26]</sup> biosensing, and intracellular detection.<sup>[27]</sup> Therefore, surface coatings derived from nGels, with the possibility of implementing the aforementioned functions, provide the opportunity to develop new advanced biomedical coatings that takes its place among the often-used polymer brush coatings and conventional hydrogel coatings. However, the nGel coating does not require complex chemistry for coating preparation as brushes and hydrogels do and can possibly be applied as a mixed system of nGels bearing several distinct but complementary functions without any effort, something that brushes and conventional hydrogel coatings would struggle with. We recently have shown such modifications by introducing quaternary ammonium groups, which has been highly effective in introducing antimicrobial properties and drug delivery capabilities both in suspension<sup>[28]</sup> and as a coating.<sup>[29]</sup> The group of Wang and co-authors demonstrated the functionalization of non-woven polypropylene-based wound dressing with polydopamine (PDA), poly(ethylene glycol) (PEG), and poly(vinylpyrrolidone) PVP–iodine to enhance the antifouling/antiadhesive and bactericidal (contact-active) properties, this resulted in  $\geq 90\%$  reduction in bacterial adhesion and diminished adhesion of red blood cells and platelets, in comparison to non-functionalized polypropylene.<sup>[30]</sup> In another strategy, Liu et al. developed a zwitterionic polymer–based coating by introducing bactericidal agent like copper (Cu) ions in contact lens to inhibit dryness in ocular region and biofilm formation.<sup>[31]</sup>

Additionally, nGel coatings have also shown to reduce the adhesion of leukocytes, adsorption of fibrinogen, and the expression of other pro-inflammatory cytokines, and hence minimize inflammatory responses in the host body.<sup>[32]</sup> These examples emphasize the potential impact of nGel-based coatings but have so far mostly been studied on glass or silicone rubber surfaces. These coatings are also highly applicable to other biomedical materials but in general, implants differ greatly in their physicochemical properties and hence applying the same nGel coating on different classes of materials is challenging. The diversity in biomaterials is large and polymeric implant materials such as polyethylene (PE), polytetrafluoroethylene (PTFE), or polymethylmethacrylate (PMMA) generally require different coating strategies than bioglass, ceramics, or metal-based implants due to the inherent difference in their chemical properties. Indeed, charge-based coatings are common and have been demonstrated before,<sup>[33,34]</sup> however, not for nGels. Previously, other coating strategies based on electrostatic interactions<sup>[34]</sup> and other non-covalent bonds have been developed as well as universal coatings based on mussel-inspired strategies<sup>[35]</sup> to create denser coatings and polymer brush layers.<sup>[33,36]</sup> However, for nGels, such approaches have not yet been developed. To enhance the coating applicability, a more relevant and better translatable universal method for coating all implants, regardless of their composition, will tremendously impact the field of biomedical coating developments (**Scheme 1**). To broadly implement a single type of functional coating, a unified approach is yet to be developed for applying the coating on a wide range of materials. This would provide the opportunity to use the coating for different applications independent of the physicochemical nature of the implant material.



**Scheme 1.** Schematic representation of the different classes of medically relevant implant materials. The spray-coating technique is a universal approach that can be applied on every class of material (bioglass/ceramic, elastomer, hard polymer, metal, fluorinated material) irrespective of their physicochemical properties. The atomic force microscopy (AFM) images show the formation of uniform and homogenous coating over the surface (partly created by biorender.com). (PDMS, polydimethylsiloxane; PVDF, polyvinylidene fluoride; PMMA, polymethylmethacrylate).

Herein, the aim of our research was to develop a universal nGel-coating approach that is suitable for as many medical materials as possible, irrespective of their diverse chemical composition and surface properties. As a conceptual proof of introducing chemical functionality, the coating was made detectable by bio-optical imaging technique using an in vivo imaging system (IVIS) and the in vitro and in vivo stability of the coating was further tested. To this end, *N*-isopropylacrylamide-*co*-*N*-(3-aminopropyl)methacrylamide dihydrochloride (p(NIPAM-*co*-APMA)) core-shell nGel particles were synthesized by free radical precipitation polymerization. Following this, the nGel-based coating was applied by electrostatically binding the positively charged particles on pre-activated plasma-oxidized surfaces to achieve a homogenous coating. Subsequently, the coating was made traceable by conjugating fluorescein isothiocyanate (FITC) to the peripheral primary amine groups for detection and imaging by IVIS. The method showed successful formation of p(NIPAM-*co*-APMA) nGel coatings on 11 different medically relevant materials from various classes with the possibility of post-labeling and good stability, without losing the implemented function. In addition to this, the tissue response toward the pNIPAM nGel coating was assessed by analyzing the early (day 7) acute phase and the chronic phase (day 13) of the foreign body reaction (FBR) toward coated polyvinylidene fluoride (PVDF) hernia meshes as compared to pristine PVDF meshes.

While the primary amine is used here for the addition of the positive charge and the possibility for post-modification, from previous works, it is eminent that many additional functionalities can be combined with nGels, which enables possible implementation in a broad range of applications as indicated earlier including antifouling,<sup>[13]</sup> antimicrobial,<sup>[28]</sup> and drug releasing<sup>[25]</sup> coatings.

## 2. Results and Discussions

### 2.1. nGel Synthesis and Coating Formation

p(NIPAM-*co*-APMA) core-shell nGel particles were synthesized via free-radical precipitation polymerization, similar as described before.<sup>[16,37]</sup> The addition of 2,2'-azobis(2-methylpropionamide)

dihydrochloride (V50) above the lower critical solution temperature (LCST) of the base monomer NIPAM allowed for the precipitation of insoluble polymeric chains, which acted as nucleation sites for the propagation of the polymerization and particle growth. The successful initiation of the synthesis was shown by the presence of the opalescence suspension, which indicated the formation of the core of the nGel.<sup>[16,38]</sup> The size of the particles was controlled by addition of the surfactant, hexadecyltrimethylammonium bromide (CTAB). Higher concentration of CTAB reduces the hydrodynamic diameter ( $D_h$ ) of the particles.<sup>[39,40]</sup> The shell of the nGel was formed by the subsequent incorporation of APMA to the mixture, which facilitated the addition of primary amine groups at the periphery of the nGel.<sup>[16,41]</sup> After the synthesis, CTAB along with other impurities was eliminated from the suspension by centrifugation and dialysis.<sup>[39]</sup>

**Figure 1** demonstrates the synthesis of the p(NIPAM-*co*-APMA) core-shell nGel. The transmission electron microscopy (TEM) images show the distinct nGel particles with a size of about  $351 \pm 25$  nm (Figure S1, Supporting Information).

Dynamic light scattering (DLS) measurements showed that the average  $D_h$  of the p(NIPAM-*co*-APMA) nGel particles at 24 °C, pH 6.2 was  $540 \pm 11$  nm (Figure S2, Supporting Information). The polydispersity index (PDI) was  $0.09 \pm 0.08$ , which indicated that it was a monodisperse colloidal suspension and contained no particle aggregates.<sup>[42]</sup> The size determined by DLS is larger than found by TEM, which can be attributed to the hydrated state for DLS and the dry state visualized in TEM.<sup>[24]</sup> The difference is slightly larger than usual between the two techniques, which could be attributed to an additional contractility due to hydrogen bonding between the primary amine groups upon drying, thereby making a denser shell while the charge repulsion of the protonation of the primary amine groups in the hydrated state expands the network.<sup>[43]</sup>

The positive charge originating from the protonated primary amine groups was shown by the zeta ( $\zeta$ ) potential, which was  $+15.8 \pm 0.1$  mV at 24 °C. The presence of cationic initiator V50 may also contribute, in addition to the amine groups, to the formation of positively charged particles.<sup>[44]</sup> The choice of monomers can be attributed to the temperature responsive

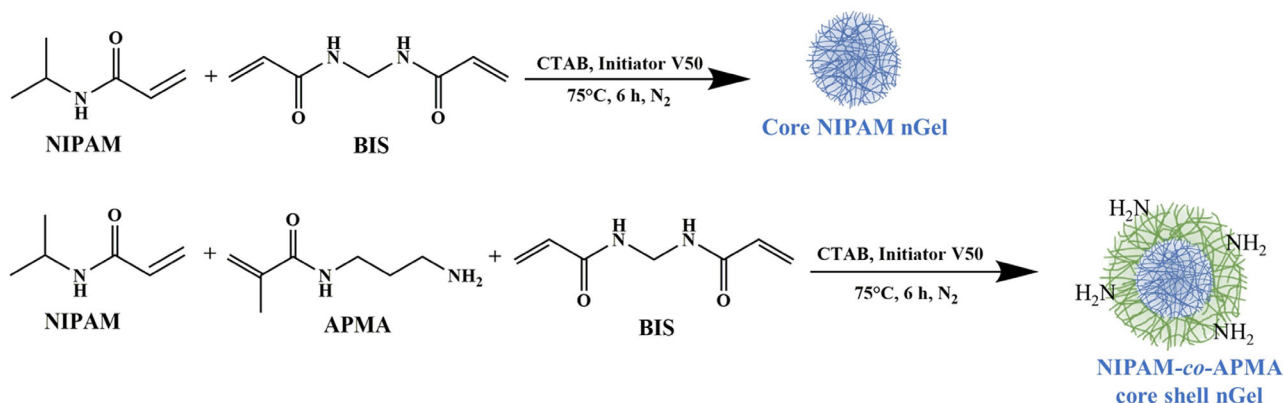


**Figure 1.** Overview of the synthesis of the nGel. The synthesis of the primary amine-functionalized nGel is done via free-radical precipitation polymerization reaction. It is a sequential process, where *N*-isopropylacrylamide (NIPAM) forms the core of the nanogel (nGel). In the successive step, the nGel is functionalized with the co-monomer *N*-(3-aminopropyl)methacrylamide (APMA) to obtain the *N*-isopropylacrylamide-*co*-*N*-(3-aminopropyl)methacrylamide dihydrochloride (p(NIPAM-*co*-APMA)) core-shell nGel.

property of NIPAM<sup>[38]</sup> whereas, APMA gives an additional primary amine to the nGel particles for fluorescence labeling.<sup>[16]</sup> Although, we have not exploited the thermosensitive character of NIPAM for the universal nGel-coating strategy, this would be an added advantage for future research in the field of drug delivery,<sup>[24,45]</sup> antifouling or antibacterial functionality.<sup>[46]</sup> The pNIPMAM nGel particles displayed a  $\zeta$ -potential of  $-16 \pm 0.4 \text{ mV}$ <sup>[29]</sup> at 24 °C and the volume-phase transition temperature (VPTT) is around 44 °C (Figure S3, Supporting Information), which ensures a hydrated state *in vivo* and is in good agreement with previously recorded values.<sup>[17]</sup>

The 1D carbon-13 cross-polarization magic angle spinning (1D <sup>13</sup>C CPMAS) nuclear magnetic resonance (NMR) spectra were recorded on the two samples, NIPAM-co-AMPA core-shell nGel and core NIPAM nGel particles, while the chemical structures are illustrated in Figure S4A, Supporting Information. Three main peaks at 25, 44, and 177 ppm, corresponding to CH<sub>3</sub>, CH<sub>2</sub> and CH, and CO groups, could be observed in both cases with no significant changes between the two samples. To overcome the limits imposed by the significant peak overlap, 2D <sup>1</sup>H-<sup>13</sup>C CP-based heteronuclear correlation (HECTOR) spectra have also been recorded (Figure S4B, Supporting Information). Few peak changes could be observed between 35 and 40 ppm. More specifically, extra broad peaks were detected at around 36 ppm in the case of the NIPAM-co-AMPA indicating the presence of the APMA block. The observed extra peaks most plausibly belong to the side chain carbon atoms of the APMA, highlighted in green in the chemical structure (Figure S4A, Supporting Information). An estimate of the percentage of the APMA in the final polymer could thus be obtained by peak deconvolution of this spectral region (Figure S4C, Supporting Information), and calculating the ratio between the value of the integral of the peak at 36.4 (<sup>13</sup>C) and 2.6 (<sup>1</sup>H) ppm and the value of the integral of the methyl peak resonating at 25.0 (<sup>13</sup>C) and 1.8 (<sup>1</sup>H) ppm. Considering that the *N,N'*-methylenebis(acrylamide) (BIS) and the APMA moiety constitute only a small fraction of the polymer (likely less than 10%), we considered that the polymer would thus contain on an average 2 methyl groups

per repeating unit (the 2 methyl groups belonging to the NIPAM). Also, we assumed that the peak resonating at 36.4 (<sup>13</sup>C) and 2.6 (<sup>1</sup>H) ppm (considered for the integration) would correspond to one single-carbon atom of the APMA side chain. So, a ratio of 2:1 CH<sub>3</sub>:CH<sub>2</sub>-APMA was considered for the normalization. By doing the peak deconvolution and integration in TopSpin, an estimate of the percentage of the APMA could be obtained, corresponding to a value of around 5%.

Upon activation of the surface of the “to be” coated material by air plasma oxidation, the surface becomes negatively charged.<sup>[47]</sup> The positively charged p(NIPAM-co-APMA) nGel particles were deposited onto the surface by a spray-coating technique and the particles were bound to the activated surface via electrostatic interactions. The coating is allowed to dry overnight at 50 °C, soon after its deposition on the implant material. The VPTT of the NIPAM-co-APMA nGel particles is close to 33 °C (data not shown), following which the particles are in their collapsed state and adheres to the surface. This ensures higher surface coverage and formation of homogenous coating on the surface.<sup>[37]</sup> Subsequently, the washing step is continued for 6 h which ensures that the multilayers/unbound particles in the coating are washed away which ultimately gives rise to a single homogeneous layer<sup>[29,46]</sup> (Figure 2). The coating on the surfaces were imaged by AFM immediately after drying the nGel-coated surfaces at room temperature, and therefore, the monolayer indicated in AFM is not due to erosion. For the *in vivo* experiments, an intermediate layer of positively charged polyethyleneimine (PEI) was introduced in between the plasma-oxidized PVDF surface and the negatively charged pNIPMAM particles. As a result, the nGel particles attached to the PEI modified mesh surface again via electrostatic interactions.<sup>[29]</sup> Additional contact angle and streaming potential experiments were performed to further identify that the charge interactions are the driving force for firm adhesion of the nGel particles and emphasize the relationship between the selected surfaces and the nGels. Figure S5, Supporting Information shows the reduction of the water contact angle after plasma oxidation, wherein the increase in the hydrophilicity of the material surface is associated with the gain of

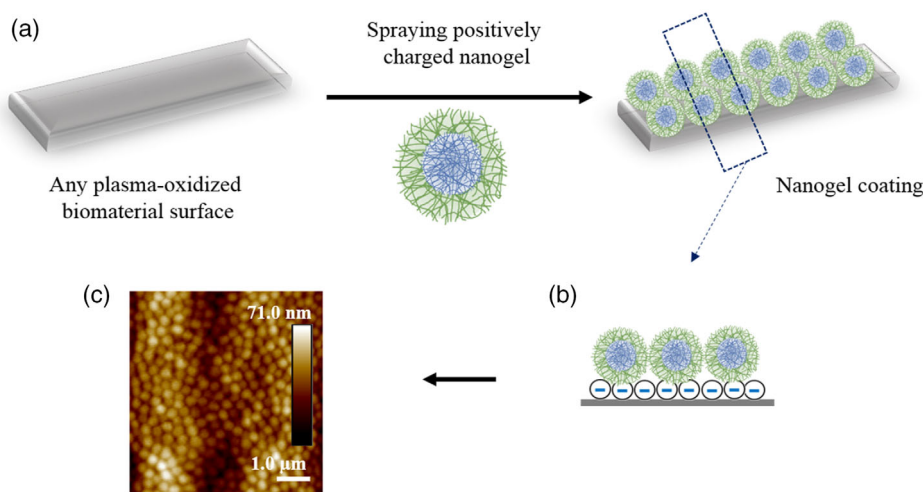


**Figure 2.** Schematic illustration of the universal nGel-based coating approach on the surface of the material. The negatively charged plasma-oxidized surface a) is spray-coated with positively charged nGel particles and attached via electrostatic interactions b) forming a dense nanogel layer c).

oxygen and, related to that, the gain of negative charge.<sup>[48,49]</sup> The exemption here is Teflon, that is known to only have moderate changes in water contact angle due to a combination of the stable nature and the excessive roughening of the surface. Therefore, for PTFE, even though there would be a moderate decrease in water contact angle, the increase in surface roughness stimulates the increase in water contact angle.<sup>[50]</sup> In addition, the increase in the negative charge attained after plasma oxidation, also for Teflon, was confirmed by the streaming potential data ( $\zeta$ -potential) for material surfaces of glass, PE, and Teflon, as shown in Table S6, Supporting Information. The increasingly negative potential of the surfaces after treatment in combination with the positive charge present at the surface of the nGel in water indicates that effective charge interactions stimulate adhesion of the nGel. Here, the size of the nGel particle was not chosen specifically, as the coating approach is not dependent on their size as we have shown previously<sup>[29]</sup> although packing might be compromised when particles become too large and can be universally applied for every particle size and on all medically relevant implant

surface. The dimensions of the particles are therefore emerging from a synthetic approach of which the reproducibility is high and previously used.<sup>[28,46]</sup> It has to be mentioned that the size of the particle could affect its function as overall coating thickness is often a parameter,<sup>[29]</sup> however not for applying the coating itself.

Previously, our group has successfully used this method for coating glass surfaces, which is very limited in terms of clinical relevancy.<sup>[29]</sup> Here, the method was further elaborated and applied as a universal approach for many different medical material surfaces in the categories: plastic (polycarbonate, polymethylmethacrylate [PMMA], PP, low-density PE), elastomer (silicone rubber, polydimethylsiloxane [PDMS]), ceramic/glass, metal (titanium and stainless steel), and fluorinated material (Teflon and PVDF). **Figure 3** shows the AFM images of the non-coated (Figure 3a1–j1) and p(NIPAM-co-APMA)-coated surfaces (Figure 3a2–j2) and Figure S7, Supporting Information demonstrates the AFM image of pNIPAM-coated glass surface in their dry state at room temperature. A closely packed nGel-layer was visible on all distinct surfaces, irrespective of their chemical

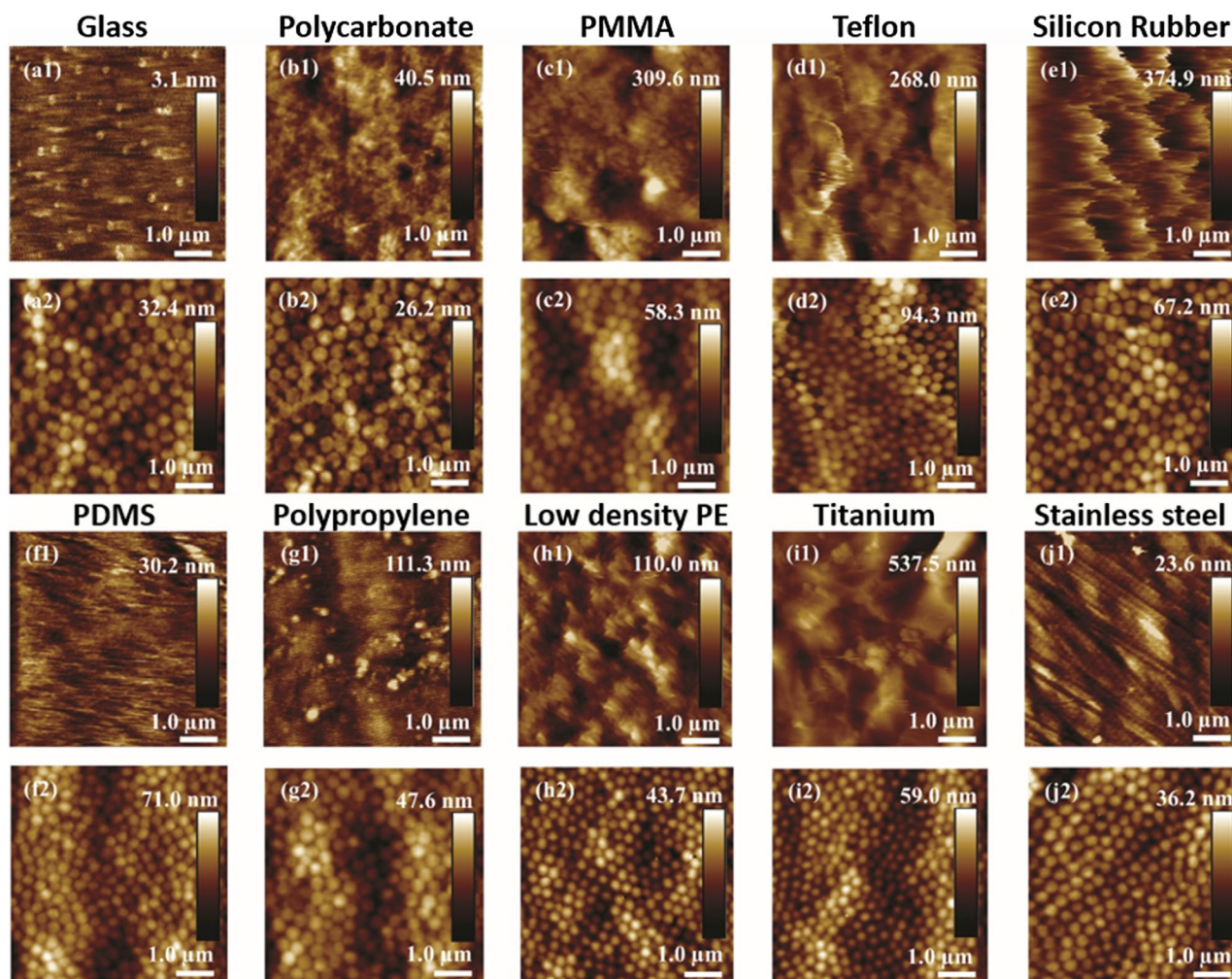


**Figure 3.** Atomic force microscopy (AFM) images captured at a scanning area of  $(5 \times 5) \mu\text{m}^2$  for the 1) non-coated and 2) p(NIPAM-co-APMA) nGel-coated materials at room temperature in the dry state: a) glass, b) polycarbonate, c) polymethylmethacrylate (PMMA), d) Teflon, e) silicone rubber, f) polydimethylsiloxane (PDMS), g) polypropylene, h) low-density polyethylene (PE), i) titanium, and j) stainless steel. (The lowest point of the height bar corresponds to 0 nm).

and structural properties. The coating covered most of the surface in a dense fashion and even the rougher surfaces display a tight packing of the nGels indicating that any pretreatments in terms of smoothening are not required for the formation of the nGel coating.

## 2.2. Post-Modification of the nGel-Coated Surfaces

Incorporation of APMA during the synthesis adds primary amines at the periphery of the nGel particles and are a general tool for many functionalization reactions under mild conditions as these methods have also been established for protein functionalization and bioconjugation reactions.<sup>[51]</sup> FITC is an amine-reactive fluorescent probe that conveniently binds to the NH<sub>2</sub> moieties by forming a thiourea functionality and is used here as a model approach.<sup>[52,53]</sup> Here, a noninvasive characterization technique, IVIS<sup>[54]</sup> was used to facilitate easy traceability of the fluorescently labeled nGel-coated surfaces. The surfaces were imaged in their dry state to avoid any background signals. **Figure 4** displays the fluorescence images captured by IVIS of the non-coated surfaces that were exposed to FITC to serve as a control for nonspecific adsorption of the reagent to surfaces, nGel-coated surfaces without (control for background signal of the nGels) and with FITC label (first, second, and third columns from the left, respectively). The materials in the first and second

column did not exhibit any appreciable fluorescence intensity, suggesting that the materials were not autofluorescent by nature and that there is no nonspecific adsorption of FITC to the material itself. The nGel-coated FITC-labeled surfaces demonstrated fluorescence signals indicating the successful conjugation between the dye and the NH<sub>2</sub> groups, a model approach for a large variety of possible modifications. While here fluorescent moieties were used, one can easily imagine the implementation of other functionalities via generally applicable peptide-like conjugation reactions.<sup>[51]</sup>

## 2.3. In Vitro Stability of p(NIPAM-co-APMA) nGel Coatings

The nGel coating provides an intermediate layer between the bare surface of the material and the biological environment.<sup>[55]</sup> Therefore, its stability is a crucial factor for any long-term application and for its translatability to the clinic. For the in vitro study, two distinct biologically relevant setups were created by exposing the nGel-coated samples to potassium phosphate saline (PBS) and fetal bovine serum (FBS) in a shaker incubator (150 rpm) to simulate a dynamic surrounding for 7, 14, and 21 days at 37 °C. As control, p(NIPAM-co-APMA) nGel-coated Teflon sample, without any exposure to PBS and FBS (Figure S8, Supporting Information), nGel-coated Teflon (**Figure 5**), and nGel-coated polypropylene, silicone rubber, and stainless steel

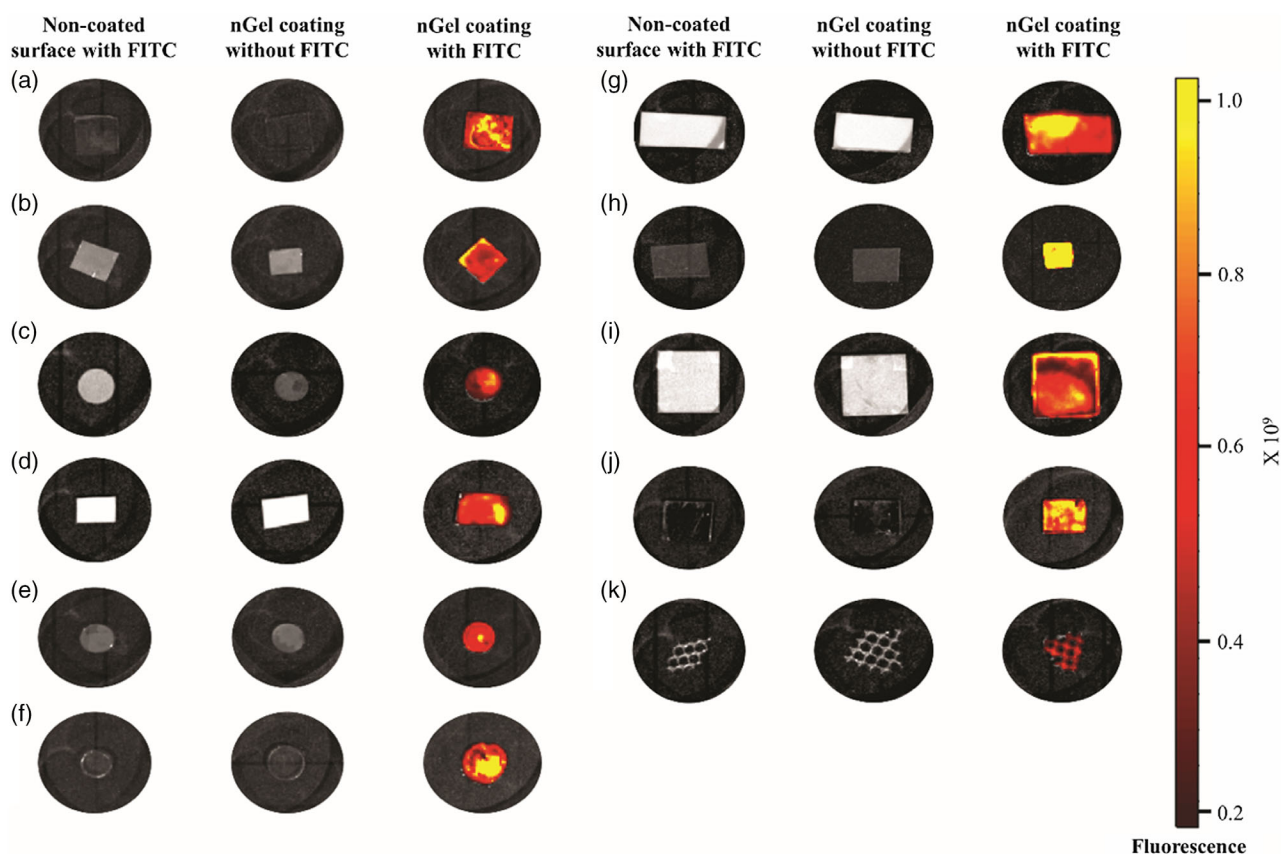


**Figure 4.** Representative fluorescence images of different p(NIPAM-co-APMA) nGel-coated surfaces captured by in vivo imaging system (IVIS), expressed in radiant efficiency ( $\text{p s}^{-1} \text{cm}^{-2} \text{sr}^{-1} / [\mu\text{W cm}^{-2}]$ ): a) glass, b) polycarbonate, c) PMMA, d) Teflon, e) silicone rubber, f) PDMS, g) polypropylene, h) low-density PE, i) titanium, j) stainless steel, and k) polyvinylidene fluoride (PVDF) surgical mesh.

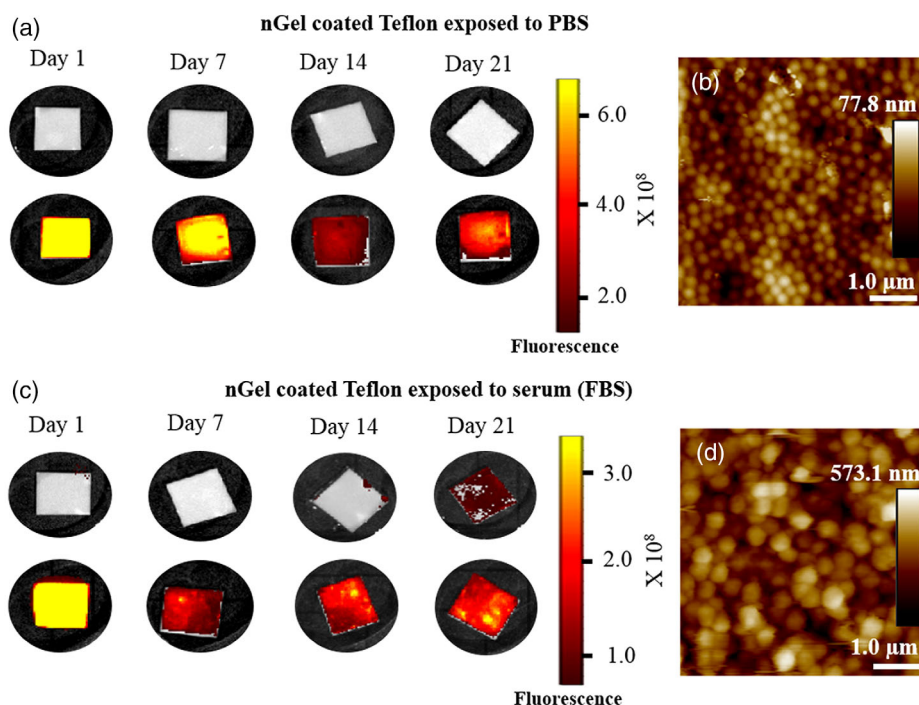


**Figure 5.** Stability test of p(NIPAM-co-APMA) nGel-coated Teflon surfaces. a) nGel-coated fluorescein isothiocyanate (FITC)-labeled Teflon exposed to potassium phosphate saline (PBS) and fluorescence images captured by IVIS at 1, 7, 14, and 21 days, expressed in radiant efficiency ( $\text{p s}^{-1} \text{cm}^{-2} \text{sr}^{-1}$ ) /  $[\mu\text{W cm}^{-2}]$ ; b) AFM image of nGel-coated Teflon exposed to PBS at day 21; c) same as (a), but now for nGel-coated FITC-labeled Teflon exposed to fetal bovine serum (FBS); d) same as (b), but now for nGel-coated Teflon exposed to FBS at day 21. (The lowest point of the height bar corresponds to 0 nm.).

(Figure S9, Supporting Information) materials were used. The temperature, salt concentration, and the pH of the system play a critical role in the stability of the coating.<sup>[56]</sup> PBS, which mimics the physiologically relevant salt concentration (maintaining an isotonic environment at pH 7.4),<sup>[57]</sup> and FBS, which mimics the human serum, containing physiologically relevant salt concentration and different proteins, were used for the study.<sup>[58–60]</sup> To compare the in vitro stability of the coating, as a control, an nGel-coated Teflon sample was kept in the shaker incubator for 21 days without any exposure to PBS and FBS (in a dry environment) and later the surface was analyzed by AFM to indicate the presence of the coating (Figure S8, Supporting Information). Teflon was used as it is the materials from which planar substrates were available that closest resembles PVDF, which was used for the in vivo stability. Upon exposure of the FITC-labeled nGel-coated Teflon surfaces to PBS, the homogeneity of the coated surface was captured by IVIS at intervals of 7, 14, and 21 days (Figure 5a). Furthermore, the persistence of the uniform layer of the coating even after 21 days was confirmed by AFM analysis (Figure 5b). Successively, the same study was performed to investigate the influence of FBS on the coated surface, while keeping all other conditions the same. The captured IVIS images at days 7, 14, and 21 show fluorescent signals indicating the presence of the coating (Figure 5c).

The presence of proteins might influence the morphology of the nGel adsorbed onto the surface as the nGels render the surface positively charged, composing the new interface. Therefore, morphological characterization of the nGel coatings

was performed by AFM after 21 days of exposure to serum. Although the coating has remained intact, its appearance in the AFM analysis indicates possible adsorption of proteins onto the surface (Figure 5d). The main component of FBS are proteins<sup>[59,60]</sup> which exhibit negative charge beyond their isoelectric point at  $\approx\text{pH } 4.5\text{--}5$ .<sup>[61]</sup> The nGel particles (suspended in ultra-pure water) indicated positive charge up to the recorded isoelectric point at  $\approx\text{pH } 10.5$ . Therefore, at physiological (neutral) pH, the negatively charged proteins may adsorb onto the positively charged nGel-coated surface via electrostatic interactions.<sup>[62]</sup> To confirm protein adsorption on nGels, the  $\zeta$ -potential of the nGels was measured after 3 h of incubation in FBS at 37 °C (Table 1). According to the results, the  $\zeta$ -potential of nGels incubated in FBS is  $-4.7 \pm 2.9$  mV, which indicates protein adsorption on the surface of the nGels. The effect of proteins on the nGel particles, when exposed to serum (FBS), was further demonstrated by recording the  $D_h$  of the particles at physiological temperature (37 °C) (Table 1) and room temperature (24 °C) (Table S10, Supporting Information). The p(NIPAM-co-APMA)

**Table 1.** Properties of p(NIPAM-co-APMA) core-shell nGel at physiological temperature (37 °C).

	$D_h$ [nm] (mean $\pm$ SD)	$\zeta$ potential [mV] (mean $\pm$ SD)
nGel suspended in water	515.2 $\pm$ 7.1	+17 $\pm$ 1.9
nGel suspended in serum (FBS)	669.1 $\pm$ 348.8	-4.7 $\pm$ 2.9



nGel particles display their VPPT at 33 °C, which lies very close to the VPPT of pure NIPAM particles (data not shown),<sup>[37]</sup> and therefore the  $D_h$  (suspended in ultrapure water) of the nGel particles reduced from  $540 \pm 1$  to  $515.2 \pm 7.1$  nm, when the temperature was increased from 24 to 37 °C, respectively (Table S10, Supporting Information and Table 1). The negative charge in  $\zeta$ -potential along with the increase in  $D_h$  ( $669.1 \pm 348.8$  nm) of the nGel particles when exposed to the proteins in FBS at 37 °C (Table 1) is also supported by the AFM image of a protein-adsorbed, nGel-coated Teflon surface (Figure 5d). Thus, on comparing the AFM images of the nGel-coated Teflon surface without exposure to any medium (Figure S8, Supporting Information) to the nGel-coated Teflon surface when exposed to PBS (Figure 5b) and FBS (Figure 5d), it can be inferred that the coating was stable under all the externally induced physiological conditions even after 21 days. The same study was also performed on polypropylene, silicone rubber, and stainless steel by exposing the coated surfaces to PBS and FBS, followed by AFM images captured at day 21 (Figure S9, Supporting Information) and similar results as for Teflon (Figure 5) were observed. The fluorescence intensity (in percentage) was quantified by taking the average radiant efficiency over 3 regions across the surface at different time intervals (Table S11, Supporting Information). The region of interests was considered around the center of the sample, as the chances of removal of the coating from the edges while human handling is always possible. Overall, a high percentage of fluorescence intensity was observed, however, the minor fluctuations in the intensity is due to the independent measurements. The deviation in the fluorescence intensity is most likely due to variation between measurements, bleaching of the dye, and material composition as there is not a continuous decrease in intensity but rather it fluctuates between timepoints and the variations are not substantial. Figure 3 also displays variations between bare materials and final coated sample, even glass of which we previously identified that the coating procedure provides a monolayer, and therefore difficult to attribute quantitative values. It was noticed that the coating was more stable when exposed to PBS than to FBS, due to protein adsorptions.

While the *in vitro* stability indicates excellent usability of the Teflon-coated surfaces, the environment *in vivo* is more complex

and hence the stability of the p(NIPMAM) nGel-coated PVDF hernia meshes were implanted subcutaneously in a mouse model (Figure 6).

The nGels used in this experiment are labeled with the methacryloxyethyl thiocarbamoyl rhodamine B (MRB) dye to be able to detect the fluorescent signal of the nGel coatings by IVIS measurements in the mouse model. As can be seen in Figure 6a, the MRB-labeled nGels presented an intense fluorescent signal on the mesh surface before the implantation in the mice.

After the implantation in the mice, the representative IVIS images have been taken on day 0, 7, and 13 and as demonstrated in Figure 6b, the fluorescence of the nGel coatings was observable at least up to 13 days *in vivo*. This short-term *in vivo* assessment can be considered as an initial proof of the stability of nGel coatings; however, further evaluation of long-term stability might also be necessary for these coatings to be used in the clinic depending on the specific application, especially combined with different surgical handling approaches.

It should be noted that the fluorophore for the mesh is very close to the autofluorescence of the fur of the mice. Thus, the fluorescence on the flanks and ears might be due to the autofluorescence of the fur.<sup>[63]</sup> In addition to the *in vitro* coating stability, the biocompatibility of these particles was previously studied,<sup>[23,24,28]</sup> which indicated low cytotoxicity.

#### 2.4. Biocompatibility of pNIPMAM-Coated PVDF Hernia Mesh

Apart from the coating stability, biocompatibility is yet another determining factor for clinical relevance. Most surgical meshes, such as PVDF hernia meshes are nonabsorbable medical implants, exhibit biocompatibility and biostability and are highly preferred for abdominal hernia surgery.<sup>[64–66]</sup> Biocompatibility often refers to the ability to reside in the host for a long time, while eliciting a low degree of inflammation and minimal fibrotic encapsulation.<sup>[13,64,65]</sup> Upon implantation, an acute inflammatory reaction occurs, which usually takes less than one week and which creates the environment for an FBR to take place. Within the chronic inflammation phase, which succeeds the acute inflammation, adhesion of monocytes, and macrophage take place followed by fusion of macrophages to form foreign

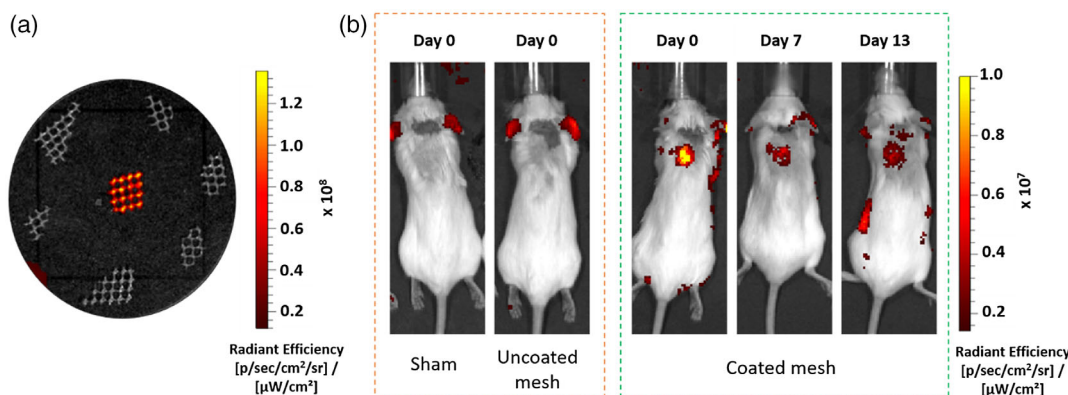


**Figure 6.** a) Representative fluorescence images of coated mesh (fluorescent color in the middle) and uncoated meshes (grey) taken by IVIS before the implantation in the mice. b) Representative fluorescence images of mouse taken without and with the uncoated PVDF mesh inside and nGel-coated PVDF meshes at different time points.

body giant cells (FBGCs), typical hall marks of the FBR.<sup>[67]</sup> Chronic inflammatory responses are succeeded after around 3 weeks by fibrotic encapsulation.<sup>[68]</sup>

That the coating is performing equally well at the pristine material is in our opinion here, a positive aspect as PVDF is known to already elicit a very minor FBR. The aim here is not to test whether the coating reduces the FBR, but whether it is biocompatible. Now that it is known that it does not elicit any strong effects, not only longer-term experiments can be safely done, but also specific functions can be introduced such as antimicrobial agents or other drugs as well as imaging modalities.

To assess the FBR to the pNIPMAM nGel coating, the acute and chronic inflammation was investigated in ex vivo samples taken 7 and 13 days after implantation of the coated and uncoated mesh after hematoxylin and eosin (HE) staining. The mesh filaments (*M*) were identified as disc-shaped openings with a diameter of  $144 \pm 18 \mu\text{m}$  ( $n = 15$ ), falling within the 85–165  $\mu\text{m}$  diameter range of the PVDF filaments (**Figure 7a**). The coated and uncoated PVDF surgical meshes along with sham were implanted inside a mouse model, which displayed an excellent stability for at least 13 days. At day 7, an influx of immune cells was identified in mice that received a coated mesh (**Figure 7a1**

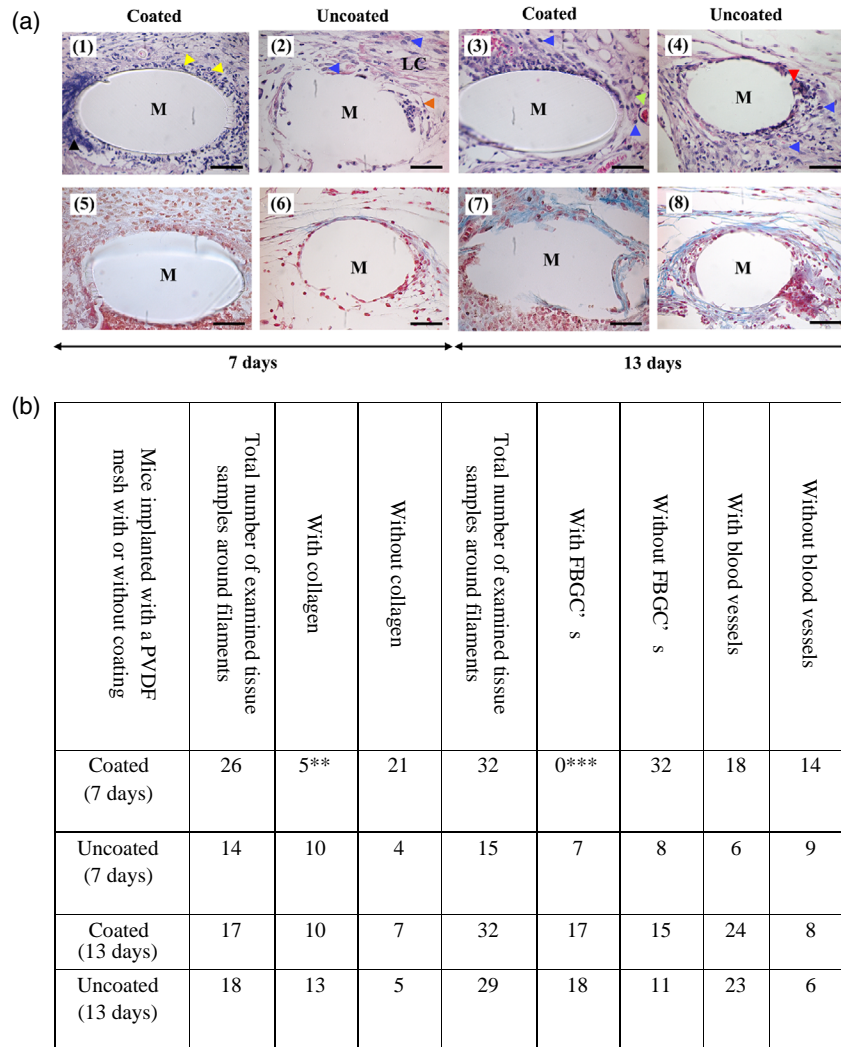


**Figure 7.** a) Representative images of hematoxylin (dark blue), eosin (pink) staining of mice tissue biopsies at positions surrounding a single filament of a pNIPMAM nGel-coated or uncoated PVDF surgical mesh implant (*M*) in combination with sterile PBS injection at 7 and 13 days after the implantation ( $n = 3$ ) at 400X magnification. Yellow arrowhead shows locations of neutrophils; orange arrowhead shows location of fibroblast-like cells; blue arrowheads show locations of macrophages; green arrowheads show locations of blood vessels and black arrowhead shows hematoxylin-stained DNA clouds. Scale bar 400X = 100  $\mu\text{m}$ . The collagen deposition is determined with Masson's trichrome stain in tissue biopsies at positions surrounding a single filament of the nGel-coated or uncoated *M* in combination with sterile PBS injection at 7 and 13 days after implantation ( $n = 3$ ). Blue color shows location of collagen bundles; red color shows location of cytoplasm and muscles (black arrowhead); pink arrowheads show locations of collagen films and brown–black color shows location of nuclei. Scale bar = 100  $\mu\text{m}$ . b) Total number of tissue samples examined around filaments with and without collagen, foreign body giant cells (FBGCs) and blood vessels in the presence and absence of a coating, evaluated on day 7 and 13, based on histology study. \*\* indicates a difference between coated and uncoated filaments with  $p = 0.002$ , \*\*\* indicates a difference between coated and uncoated filaments with  $p = 0.0001$  (two-sided Fisher exact test, GraphPad PRISM 9).

blue hematoxylin-stained nuclei). These immune cells mainly consisted of neutrophils, as identified by their irregular nuclei (Figure 7a1, yellow arrowheads). Blood vessels and clouds of hematoxylin-stained DNA (Figure 7a1, black arrow) were discovered near the coated filaments, while no FBGCs were identified. At day 7, a lower immune cell infiltration was present in the group of mice that received an uncoated mesh implant (Figure 7a2) in comparison to tissues surrounding the coated mesh (Figure 7a1). Tissue surrounding the filament in the uncoated mesh consisted of loose connective (LC) tissue scattered with possibly macrophages (blue arrowheads) and fibroblast-like cells (orange arrowhead), as identified by their round nuclei and elongated morphology (Figure 7a2). Also, FBGCs and blood vessels were identified in the vicinity of the mesh filaments. At day 13, the acute inflammation has now evolved into the chronic inflammation. At this stage, low inflammatory cell infiltration was seen around both coated and uncoated filaments in mice (Figure 7a3,a4), with mainly macrophages (blue arrowheads) and the tissue consisting of LC tissue. Blood vessels (single layer of endothelial cells surrounding red eosin-stained erythrocytes, green arrowhead, Figure 7a3), as well as FBGCs (red arrowhead, Figure 7a4), were recognized near coated and uncoated filaments. FBGC's and collagen formation were assessed in the acute and chronic inflammation phase since both are hallmarks of the early and chronic FBR, respectively.

Therefore, biopsies of tissue around the filaments were taken from both groups of mice and were stained blue with Masson's trichrome staining (Figure 7) to obtain a measure of collagen deposition. At day 7, there was low collagen deposition in the coated (Figure 7a5, blue stain) and uncoated mesh (Figure 7a6, blue stain). However, collagen fibers were identified more frequently around-uncoated (10 out of total 14 examined tissue samples around filaments) than around-coated mesh filaments (5 out of total 26 examined tissue samples around filaments) (Figure 7a6). Remarkably, all collagen fibers aligned perpendicular to filaments at day 13, higher collagen percentages (10 out of total 17 and 13 out of total 18 examined tissue samples around filaments for coated and uncoated PVDF meshes, respectively) were found positive in aligned collagen bundles (Figure 7a7, a8), although differences were not significant. Our results indicated that the pNIPAM coatings affected the FBR around the filaments, particularly, in the acute inflammation phase. Adhesion of macrophages is a prerequisite for the formation of FBGCs and can be influenced by material surface properties.<sup>[69,70]</sup> Possibly, this is a consequence of the prevention of macrophage adhesion by the hydration layer formed by the pNIPAM nGel coating, as previously reported for other hydrophilic coatings such as hyaluronic acid<sup>[71]</sup> and poly(sulfobetaine methacrylate).<sup>[72,73]</sup> Although, the reduced collagen formation observed after 7 days around filaments in the presence of the coating (table in Figure 7b) might indicate the possibility of reduced fibrotic capsule formation associated with collagen fibers, this was not corroborated by the collagen deposition in the chronic inflammation phase.<sup>[74,75]</sup> This was in line with the higher number of FBGCs in the chronic phase, since FBGCs are responsible for secreting cytokines that stimulate collagen deposition by fibroblasts. Additionally, the number of blood vessels, recorded in the table in Figure 7b, indicated that the coated filaments started to induce neovascularization earlier than the non-coated filaments, which was also observed earlier in poly(carboxybetaine methacrylate) hydrogels pointing to early healing.<sup>[68]</sup>

In the spectrum of immunogenic biomaterials, PVDF exhibits low immune response compared to other clinically relevant implant materials, like polypropylene,<sup>[64]</sup> when used in hernia mesh systems. Our research has shown that the application of the pNIPAM coating on the PVDF hernia meshes started to have considerably reduced its immunogenicity at the acute phase, whereas, no significant differences between the non-coated and nGel-coated PVDF meshes were observed at day 13. This suggests that application of nGel coating is not aggravating the FBR, anticipating that the fibrotic encapsulation will be comparable to the pristine surface. Nevertheless, the fibrotic encapsulation should be assessed rather over a longer period of time (e.g., after 3 months) than just during the acute and chronic phase and with a more diverse range of implantable materials. Currently, it seems justified to state that the nGels are of equal biocompatibility as PVDF, already a low FBR eliciting material, and it would be interesting to utilize biomaterials that are known to induce a stronger FBR and compare.

### 3. Conclusions

In this study, the goal was to develop a uniform coating mechanism that addresses a large number of unique material surfaces, regardless of their physicochemical properties and furthermore, and to study the stability (in vitro) and biocompatibility (in vivo) of the coating on different implant surfaces. This innovative nGel coating was successfully translated to all the 11 unique medically relevant materials; hence, we call it a universal coating approach. It is a straightforward method, time efficient, inexpensive, and highly reproducible. The homogeneity of the nGel-coated surfaces was indicated by the AFM images. As a proof of concept, the coating was labeled with FITC and the emission of the fluorescent signals indicated the successful binding between the primary amines present in the periphery of the nGel and the thioisocyanate of the dye. We have established that the nGel-based coatings applied on diverse range of materials exhibit remarkable stability when exposed to in vitro (in PBS and FBS solutions, at body temperature and dynamic conditions). In vivo experiments were conducted in mice and the tissue response to coated and uncoated PVDF was similar, specifically at day 13, marked by equivalent immune cell infiltration, FBGC formation, collagen deposition, and formed blood vessels. It can therefore be concluded that the pNIPAM-based nGel-coated PVDF mesh is as biocompatible as pristine PVDF.

In the future, different functions such as, antifouling, antibacterial properties, anticancer drugs, or imaging modalities can be incorporated into the coating, thereby creating a highly functional and potentially multimodal system depending on the desired biomedical application. Since the coating approach is no longer limited to a specific material, translation toward a broad range of applications is possible, the main feature being the universal approach. Moreover, translation toward the clinic can also be very broadly explored.

### 4. Experimental Section

*Materials:* Monomer, N-isopropylacrylamide (>98%, NIPAM) was purchased from Tokyo Chemical Industry (TCI), Belgium, and the

co-monomer *N*-(3-aminopropyl)methacrylamide dihydrochloride (>98%, APMA) and MRB dye were obtained from Polysciences, Inc., Germany. Monomer, pNIPAM (97%), the cross-linker BIS (99%), surfactants CTAB (>99%), and sodium dodecyl sulfate, initiators V50 (97%), and ammonium persulfate (98% APS), FITC dye (>90%), and PEI (branched, Mw 25 000 g mol<sup>-1</sup>) were purchased from Sigma–Aldrich, The Netherlands. NIPAM was recrystallized from hexane; all other chemicals were used as received without any further purification. For all the experiments, ultrapure water was used (18.2 MΩ, arium 611 DI water purification system; Sartorius AG, Germany).

A range of commercially available medical implant materials were employed for the experimental study and used for applying the nGel coating: glass, polycarbonate, Teflon, PMMA, silicone rubber, PDMS, polypropylene, low-density PE, titanium, stainless steel, and PVDF mesh. Glass was obtained from Thermo Scientific Menzel–Gläser (Gerhard Menzel B.V. & Co. KG, Braunschweig, Germany), the PVDF surgical mesh was obtained from a textile implant Dynamesh Endolap PVDF, (FEG Textiltechnik GmbH, Aachen, Germany), and PDMS was prepared in the laboratory by using SYLGARDTM 184 silicone elastomer base and silicone curing agent (Dow Europe GMBH C/O Dow Silicones Deutschland GMBH, Weisbaden, Germany) in the ratio of 10:1 by weight. The rest of the materials were obtained from the Research Instrument Laboratory at the University Medical Centre Groningen (UMCG).

**Synthesis of p(NIPAM-co-APMA) and pNIPAM Core–Shell nGel:** p(NIPAM-co-APMA) core–shell nGel is a one-step copolymerization reaction. The reaction was carried out in a 100 mL three-necked round-bottom flask, attached to a water-jacketed condenser, a thermometer and an inlet/outlet for nitrogen. The first solution (main solution) was prepared by dissolving NIPAM (754 mg, 6.66 mmol), BIS (53.8 mg, 0.34 mmol), and CTAB (2.4 mg, 0.006 mmol) in ultrapure water (45 mL). The mixture was purged with nitrogen to remove any traces of oxygen for 30 min at 75 °C. Subsequently, the reaction was initiated by adding solution 2, which is, degassed aqueous solution (5 mL) of V50 (27.1 mg, 0.09 mmol) in a dropwise manner. After 10 min, the suspension transformed from clear to a milky-turbid suspension, indicating successful initiation of the reaction. Meanwhile, solution 3 was prepared separately by dissolving NIPAM (337 mg, 2.97 mmol), APMA (62.8 mg, 0.35 mmol), BIS (26.4 mg, 0.17 mmol), and CTAB (1 mg, 0.002 mmol) in ultrapure water (25 mL) and was degassed for 30 min; thereafter, the mixture was immediately injected (dropwise) into the main solution, while the synthesis was performed under nitrogen atmosphere at 75 °C. After 6 h, the reaction was allowed to cool to room temperature and removing the constant nitrogen supply while continuing with overnight stirring.

For purification, the suspension was centrifuged (38 352 g) for 1 h; subsequently, the supernatant was removed and the particles were washed in ultrapure water 3 times. Subsequently, it was dialyzed (molecular weight cutoff 3500 Da) against ultrapure water by replacing the water twice per day, for 3 days. Later, the suspension was freeze-dried and the final product, p(NIPAM-co-APMA) core–shell nGel, was stored at room temperature for later use.

For the *in vivo* experiment, pNIPAM nGel particles were used. In *in vivo* conditions, the hydrogel would preferably be in its hydrated state, pNIPAM has a VPTT of 44 °C, meaning that it remains in its hydrated state while pNIPAM would be collapsed (hydrophobic) above 32 °C. The pNIPAM nGels were prepared by precipitation polymerization, as previously described.<sup>[29]</sup> Briefly, pNIPAM (626 mg), BIS (12 mg) and of MRB (10 mg) was dissolved in ultrapure water (45 mL) using a three-necked 100 mL flask equipped with a flat anchor-shaped mechanical stirrer and a reflux condenser. The reaction mixture was degassed with N<sub>2</sub> for 1 h. The solution was heated till 70 °C and the reaction was started by injecting the degassed initiator solution APS (11 mg) in ultrapure water (5 mL) into the reaction mixture. The reaction was continued for another 4 h at 70 °C and 300 rpm under N<sub>2</sub> atmosphere. After 4 h, the reaction mixture was cooled to room temperature and stirred overnight. The nGel dispersion was purified by ultracentrifugation and washed with ultrapure water (3 times at 179 200 g). The final product (pNIPAM nGel) was freeze-dried after purification for further use.

**nGel-Coating Formation:** For the coating procedure, a previously used approach was used by us.<sup>[29]</sup> Briefly, the surface of the materials was cleaned by 70% ethanol, followed by ultrapure water and dried with pressurized air. The surfaces were air plasma oxidized for 10 min (100 mTorr and 0.2 mbar, on Plasma Active Flecto 10 USB) and immediately spray-coated with nGel suspension. This nGel suspension (5 mg mL<sup>-1</sup>, 0.5 wt%) was prepared and sonicated for 10 min (Transsonic TP690, Salm en Kipp B.V., the Netherlands) to break any particle agglomeration. In the next step, the spraying device was tilted at 45° to spray-coat the entire surface exposed to air plasma. The spraying apparatus was a glass bottle equipped with a spray nozzle that helped to convert the nGel suspension into a spray. The suspension was dispensed with each spray burst (140 µL) and it was continued until the surface was wetted completely. The coated surface was dried at room temperature for 2 h and later kept in the oven at 50 °C, overnight. To remove the excess (multi-layered) dried nGel from the coated surface, it was immersed in ultrapure water for 6 h, while the water was replaced for 3 times, to obtain a homogenous monolayer coating on the surface. For the *in vivo* experiments, PVDF hernia meshes were cleaned, dried, and placed in a sterile cabinet, as described earlier. In the following step, the meshes were plasma oxidized (under the same conditions), later immersed in a solution of PEI (1.5 mg mL<sup>-1</sup>, 0.15 wt%) for 20 min while the pH of the solution was adjusted to pH 7 with 0.1 M HCl. The PEI-coated meshes were rinsed 3 times with ultrapure water and dried at room temperature. The pNIPAM nGel suspension (5 mg mL<sup>-1</sup>, 0.15 wt%) in water was sprayed on both sides of the PEI-coated meshes until the entire surface was wetted by the coating. The same drying and washing procedure was followed, as previously mentioned.

**Post-Modification of p(NIPAM-co-APMA) nGel Coating:** FITC solution was prepared by dissolving (10.14 mg, 26 mmol) in ultrapure water (2 mL). All the materials were placed in 6 wells plates. First, the surfaces were fully submerged in 2 mL water, and subsequently, FITC solution (25 µL) was added to each well. The plates were covered with aluminum foil and kept on a shaker for 2 h at 300 rpm. The FITC-labeled surfaces were washed with water (to remove the excess dye) and dried at room temperature. Fluorescence images were taken by IVIS (IVIS Lumina II, PerkinElmer) for a exposure time of 1 s in the dry state and analyzed by Living Image software at the excitation wavelength of 465 nm and emission wavelength of 520 nm (green fluorescent protein; GFP range). Fluorescence images were taken and automatically corrected for background noise.

**In Vitro Stability Test of p(NIPAM-co-APMA) nGel Coating on Different Implant Surfaces:** *In vitro* stability tests were performed with PBS (10 mM PBS, 0.15 M NaCl, pH 7.4) and FBS (diluted to 10% with physiological salt (0.9 % w/v of NaCl)). Teflon surfaces coated with p(NIPAM-co-APMA) nGels were placed for up to 21 days in PBS and FBS in well plates on a shaker incubator with 150 rpm of speed, both at 37 °C. As a reference, nGel-coated Teflon surfaces were also placed in the same incubator without exposure to any medium (dry environment) on the surfaces at 37 °C. All nGel-coated Teflon pieces were sterilized before use by dipping in 70% ethanol for 5 min and afterward washed excessively using sterilized ultrapure water before the stability tests. The PBS and FBS media were refreshed twice weekly in a sterile hood aseptically. For IVIS and AFM measurements, slides were immersed for 10 min in sterile ultrapure water. IVIS images were taken after an interval of 7, 14, and 21 days of PBS and FBS exposure. Prior to AFM imaging, slides were dried for 30 min in ambient air, and morphological characterization of the nGel coatings was performed by AFM measurements after 21 days of exposure to PBS and FBS (see following sections for details).

**Animals, Surgical Procedure, and Imaging:** Permission for the animal experiment was granted by the competent authority (Centrale Commissie Dierproeven, CCD, Den Haag, The Netherlands) (IvD protocol 197 305-01-001), and animals were treated according to those guidelines. Female Balb/c OlaHsd mice of 4–5 weeks and an average weight of 20 g were used. After implantation, all mice were inspected every 2 days, noting any anomalies in behaviors, appearance of the skin and wound, and measuring weight. Humane endpoints were established in advance, including signs of apathy, weight loss >15% from the starting weight, pus excretion from any wound, or redness and/or swelling around the implantation site for more than 4 days. When any endpoint was met, animals were

terminated. Animals were anesthetized with 2% isoflurane gas during the experimental procedure.

At  $T = 0$  ( $T = \text{day}$ ), the skin was sterilized with chlorhexidine and shaved. The 1 cm incision was made in the mouse's dorsal cervical area and a subcutaneous pocket was created in the caudal direction in which a sterile 1 cm<sup>2</sup> PVDF mesh with or without an nGel coating was inserted. For the sham group, the procedure was identical except that no mesh was inserted. The wounds were closed with Histoacryl. Finally, Temgesic (Indivior UK Limited, UK) (0.05 mg kg<sup>-1</sup>) was administered subcutaneously for pain relief.

Three groups of mice were created: 1) group with coated mesh ( $n = 4$  for day 7,  $n = 3$  for day 13), 2) group with uncoated mesh ( $n = 4$  for day 7,  $n = 3$  for day 13), 3) group with sham surgery ( $n = 3$  for both day 7 and 13).

At day 7 and day 13, the meshes and the surrounding tissues were collected from the subcutaneous pockets under anesthesia. Each sample was fixed overnight in 4% paraformaldehyde at 4 °C, dehydrated using a series of ethanol in ascending concentrations (70%, 80%, 90%, 100%), washed with xylene and embedded in paraffin for histological analysis.

Fluorescence was measured using IVIS imaging at 0, 7, and 13 days post-implantation to investigate the stability of the pNIPMAM nGels on the mesh surface. The fluorescence signal of the uncoated and coated meshes in the animal models was measured with the IVIS Spectrum system using the spectral unmixing function of the complementary Living Images 4.7.2 software (PerkinElmer). All animals were sedated using 2% isoflurane gas inhalation during imaging. When measuring fluorescence a series of measurements was taken, all with imaging time 1.5 s, binning factor 8, field of view 21.2 cm, and emission/excitation filters set to 660/605, 680/605, 700/605, 720/605, 740/605, 760/605, 780/605, 680/640, 700/640, 720/640, 740/640, 760/640, and 780/640, respectively. Data was analyzed using the same software. The mice were terminated using cervical dislocation, after retrieving the tissue samples using the previously described anesthetic procedure (2% isoflurane gas).

**Histological Analysis:** All staining procedures were performed on 5  $\mu\text{m}$  thick slices that were cut from the paraffin-embedded samples. The slices were deparaffinized in xylene (EMSURE, Darmstadt, Germany) for 10 min. Followed by ethanol rehydration steps in descending concentrations of ethanol (100%, 96%, 70%). After washing in demineralized water, HE staining was executed. Therefore, slices were stained with Mayer's hematoxylin (Sigma, ST. LOUIS, USA) for 5 min and washed several times with demineralized water and tap water to develop the blue color of the stain. Afterward, eosin (Eosin Y) was performed for 40 s, after which the samples were dehydrated and incubated in xylene. Finally, the slices were covered with Permount mounting medium (Fisher Scientific, New Jersey, USA) and a glass cover slip and allowed to dry overnight in a fume hood at room temperature. Images were obtained with a bright-field light microscope.

For collagen determination, Masson's trichrome staining was performed. The 5  $\mu\text{m}$  slices of paraffin-embedded tissues from mice with uncoated or p(NIPMAM)-coated PVDF meshes, were deparaffinized and rehydrated, as described earlier. The samples were stained for 10 min in Weigert's hematoxylin solution to stain nuclei brown-black. The hematoxylin stain was developed in running tap water for 10 min. Next, the slices were washed in demineralized water. The samples were then incubated in Biebrich scarlet-acid fuchsin (Sigma-Aldrich, Darmstadt, Germany) for 12 min. This step was followed by incubating the slices in a 1:1 mixture of phosphomolybdic (Sigma-Aldrich) and phosphotungstic acid (Sigma-Aldrich) for 12 min which stained collagen, connective tissue, and cytoplasm red. This step was followed by incubating the slices in decolorizing agents, a 1:1 mixture of phosphomolybdic (Sigma-Aldrich) and phosphotungstic acid (Sigma-Aldrich), for 12 min. Collagen bundles were stained blue after incubating in aniline blue (Sigma-Aldrich) for 10 min. After washing with demineralized water, the slices were dehydrated in increasing concentrations of ethanol (70%, 96%, 100%) and finally a 6 min incubation in xylene, both at room temperature. The slices were covered with Permount mounting medium and covered with a glass cover slip and allowed to dry overnight at room temperature in a fume hood. Images were obtained with a bright-field light microscope. For quantitative analysis of the blue collagen stain, a blue filter of a home-made

software was used to isolate the blue stain of collagen in acquired bright-field images. Afterward, the mean gray value was determined with imagej.

**Statistical Analysis:** Statistical evaluation was performed with Graphpad Prism 9 (Graphpad, San Diego, United States). Statistical analysis was done using the two-sided Fisher exact test \*\*difference between coated and uncoated filaments with  $p = 0.002$  and the \*\*\*difference between coated and uncoated filaments with  $p = 0.0001$ .

**DLS and Zeta Potential:** The electrophoretic mobility and PDI of both the nGel particles were quantified at 24 °C, while the temperature-independent hydrodynamic diameter ( $D_h$ ) of p(NIPAM-co-APMA) nGel particles were recorded at 24 °C and temperature-dependent readings of the hydrodynamic diameter ( $d_h$ ) of pNIPMAM nGel particles were recorded by varying the temperature range from 24 to 64 °C at intervals of 2 °C by ZetaSizer Nano-ZS equipment (Malvern Instruments, Worcestershire, UK). For the measurements, the nGel suspension was diluted in ultrapure water (0.5 mg mL<sup>-1</sup>) to avoid multiple scattering and the nGel suspension pH was 6.2. The size of the particles was measured in a disposable cuvette. The instrument was operated at a steady scattering angle of 173° using a laser beam of wavelength 633 nm. The data was computed by cumulant fit analysis and the  $D_h$  was calculated by implementing the Stokes-Einstein equation by the software.

The electrophoretic mobility of the particles was quantified using a disposable folded capillary cell, at an angle of 17° and a laser beam of wavelength 633 nm. The  $\zeta$ -potential was determined from the electrophoretic mobility of the particles by applying the Smoluchowski equation. The final collected data of the size, PDI, and  $\zeta$ -potential of the particles is the average of three consecutive measurements of the same sample.

To determine the protein formation on nGels, the  $\zeta$ -potential and size measurements were performed after 3 h of incubation in FBS at 24 and 37 °C.

**Solid-State Nuclear Magnetic Resonance:** The solid-state nuclear magnetic resonance (ssNMR) was performed on a Bruker Avance Neo Fourier transform-NMR spectrometer equipped with a standard bore 14.1 T magnet and a 3.2 mm EFree HCN CPMAS probe from Bruker Biospin. The Larmor frequencies were 600.3 MHz (<sup>1</sup>H), 150.9 MHz (<sup>13</sup>C), and 60.8 MHz (<sup>15</sup>N). The <sup>1</sup>H and <sup>13</sup>C chemical shifts were referenced to aqueous 2,2-dimethyl-2-silapentane-5-sulfonic acid (DSS) using the indirect method, by measuring the adamantane <sup>13</sup>C signals.<sup>[76]</sup> The 1D <sup>13</sup>C cross-polarization (CP) magic-angle-spinning spectra were acquired under the following conditions: <sup>1</sup>H 90° pulse was set to 2.5  $\mu\text{s}$  corresponding to a radiofrequency (rf) of  $\approx 100$  kHz; the CP step was performed with an optimized contact time (CT) for maximum polarization transfer of 2000  $\mu\text{s}$  using a 70%–100% ramped-amplitude (RAMP) shape at the <sup>1</sup>H channel and using a 50 kHz square-shape pulse on the <sup>13</sup>C channel; recycle delay was 4 s. During acquisition, a two-pulse phase-modulated (TPPM) decoupling scheme was employed using a pulse length for the basic decoupling units of 4.8  $\mu\text{s}$  at rf field strength of  $\approx 100$  kHz.<sup>[77]</sup> The 2D <sup>1</sup>H-<sup>13</sup>C Lee-Goldburg (LG)-CP HECTOR spectra were acquired using Frequency-Switched Lee-Goldburg (FSLG) <sup>1</sup>H homonuclear decoupling during the indirect dimension (t1).<sup>[78]</sup> LG-CP was employed to achieve <sup>1</sup>H to <sup>13</sup>C magnetization transfer, using CT of 2000  $\mu\text{s}$ , <sup>13</sup>C rf amplitude of  $\approx 50$  kHz and 4 s recycle delay. The 158 t1 points with 32 scans each were recorded. A <sup>1</sup>H rf field strength of 100 kHz and symmetric LG offsets of 70 711 and -70 711 Hz were used for FSLG decoupling employing a LG pulse of 8.17  $\mu\text{s}$ . Quadrature detection in t1 was achieved by the States-TPPI method. The ssNMR spectra were processed and deconvoluted using TopSpin 4.07.

**Transmission Electron Microscopy:** The morphology of the nGel particles were captured by Philips CM120 microscope fitted to a 4 k CCD camera with an acceleration voltage of 120 kV. The samples were drop-casted on a carbon film-coated with copper grid and then negatively stained by uranyl acetate.

**Atomic Force Microscopy:** The surface topography of the coated surfaces was visualized by AFM (Dimension 3100 Nanoscope V, Veeco, Plainview) in the dry state. The measurements were performed using a Bruker model DNP-10 tip (made of non-conductive silicon nitride, spring constant of 0.24 N m<sup>-1</sup>) in contact mode over a scanning area of 5  $\times$  5  $\mu\text{m}^2$  of the

non-coated and coated surfaces. All the data were evaluated by NanoScope Analysis (version 1.80) software.

**Streaming Potential:** The streaming potential of glass, Teflon, and PE (75 × 26 × 1 mm) was measured by flowing an electrolyte, potassium chloride (KCl) solution (10 mM) through a home-made parallel flow chamber device. Platinum electrodes (5 × 25 mm) were present at both ends of the flow chamber to determine the potential difference across the surface at different pressure points, ranging from 37.5 to 150 Torr, and each pressure was applied for 10 s from alternate directions for a total of 6 min. The final data was obtained from three consecutive independent measurements before and after plasma oxidation of the surfaces.

**Water Contact Angle:** The wettability of the surface of the materials was measured by the sessile drop technique at room temperature. Droplet of ultrapure water (1–1.5 µL) was placed on the surface before and immediately after the plasma oxidation. Measurements were taken using an in-house built contour monitor while the images were captured using MATLAB program.

## Supporting Information

Supporting Information is available from the Wiley Online Library or from the author.

## Acknowledgements

D.G., D.K., and A.M.F. contributed equally to this work. The authors acknowledge the financial support of the Graduate School of Medical Sciences (GSMS) of University Medical Centre of Groningen, the Netherlands, the European Union's Horizon 2020 research and innovation program under the Marie Skłodowska–Curie grant agreement no. 713482 (ALERT Cofound), the China Scholarship Council (CSC no.201706890012), and by the personalized implants ecosystem made possible by the European Regional Development Fund (ERDF), coordinated by SNN, with co-financing from the Municipality of Groningen and the Ministry of Economic Affairs and Climate. The authors thank Willem Woudstra for the discussions and help of IVIS analysis of the animal images, Joop de Vries for technical help related to AFM, and Hans Kaper for training and technical help on streaming potential.

## Conflict of Interest

P.V.R. also is co-founder, scientific advisor, and share-holder of BiomACS BV, a biomedical oriented screening company. The authors declare no other conflict of interests.

## Author Contributions

D.G.: has performed major experiments and written the manuscript. A.M.F., C.W.K.R., and R.B.: have performed and analyzed the animal experiments. D.K., C.M.S., and G.Z.: have provided assistance in experimental analysis. A.L. and P.C.A.V.D.W.: have performed the ssNMR spectroscopy analysis. D.K., T.G.V.K., M.J.H.W., J.S., H.C.V.D.M., and P.V.R.: have supervised the research. P.V.R.: has conceptualized the study. All the authors have agreed to the final version of the manuscript.

## Data Availability Statement

The data that support the findings of this study are available from the corresponding author upon reasonable request.

## Keywords

biocompatibility, coatings, hydrogels, medical implants, nanogels, spray deposition

Received: September 6, 2022

Revised: February 22, 2023

Published online: April 19, 2023

- [1] Y. Li, W. Chen, L. Lu, *ACS Appl. Bio Mater.* **2020**, 4, 122.
- [2] S. Bhat, A. Kumar, *Biomatter.* **2013**, 3, e24717.
- [3] H. P. Suzie, M. E. Davis, *Bioconj. Chem.* **2002**, 13, 630.
- [4] A. S. Piotrowski-Dispit, A. C. Kauffman, L. G. Bracaglia, W. M. Saltzman, *Adv. Drug Delivery Rev.* **2020**, 156, 119.
- [5] R. Stoop, *Injury* **2008**, 39, 77.
- [6] M. Yanez, J. Blanchette, E. Jabbarzadeh, *Curr. Pharm. Des.* **2017**, 23, 6347.
- [7] N. Martins, C. F. Rodrigues, *J. Clin. Med.* **2020**, 9, 722.
- [8] B. N. Brown, S. F. Badylak, in *Regenerative medicine applications in organ transplantation*, Elsevier Inc., Amsterdam **2014**, pp. 151–162.
- [9] S. Gupta, H. Gupta, A. Tandan, *Natl. J. Maxillofac. Surg.* **2015**, 6, 3.
- [10] H. I. Sussman, A. R. Volker, in *Mini Dental Implants: Principles and Practice*, Elsevier Inc., Amsterdam **2013**, pp. 101–116.
- [11] S. Raikar, P. Talukdar, S. Kumari, S. K. Panda, V. M. Oommen, A. Prasad, *J. Int. Soc. Prev. Community Dent.* **2017**, 7, 351.
- [12] A. Nouri, C. Wen, in *Surface Coating and Modification of Metallic Biomaterials*, Elsevier Inc., Amsterdam **2015**, pp. 3–60.
- [13] D. Keskin, G. Zu, A. M. Forson, L. Tromp, J. Sjollem, P. Van Rijn, *Bioact. Mater.* **2021**, 6, 3634.
- [14] M. Molina, M. Asadian-Birjand, J. Balach, J. Bergueiro, E. Miceli, M. Calderón, *Chem. Soc. Rev.* **2015**, 44, 6161.
- [15] Y. Sasaki, K. Akiyoshi, *Chem. Rec.* **2010**, 10, 366.
- [16] W. H. Blackburn, L. A. Lyon, *Colloid Polym. Sci.* **2008**, 286, 563.
- [17] S. Schmidt, M. Zeiser, T. Hellweg, C. Duschl, A. Fery, H. Möhwald, *Adv. Funct. Mater.* **2010**, 20, 3235.
- [18] Y. Yin, B. Hu, X. Yuan, L. Cai, H. Gao, Q. Yang, *Pharmaceutics* **2020**, 12, 290.
- [19] J. Yin, D. Dupin, J. Li, S. P. Armes, S. Liu, *Langmuir* **2008**, 24, 9334.
- [20] S. Schimka, Y. D. Gordievskaya, N. Lomadze, M. Lehmann, R. Von Klitzing, A. M. Romyantsev, E. Y. Kramarenko, S. Santer, *J. Chem. Phys.* **2017**, 147, 031101.
- [21] O. Mergel, S. Schneider, R. Tiwari, P. T. Kühn, D. Keskin, M. C. A. Stuart, S. Schöttner, M. de Kanter, M. Noyong, T. Caumanns, J. Mayer, C. Janzen, U. Simon, M. Gallei, D. Wöll, P. Van Rijn, F. A. Plamper, *Chem. Sci.* **2019**, 10, 1844.
- [22] D. M. Eckmann, R. J. Composto, A. Tsourkas, V. R. Muzykantov, *J. Mater. Chem. B* **2014**, 2, 8085.
- [23] L. Ribovski, E. de Jong, O. Mergel, G. Zu, D. Keskin, P. Van Rijn, I. S. Zuhorn, *Nanomed. Nanotechnol. Biol. Med.* **2021**, 34, 102377.
- [24] G. Zu, O. Mergel, L. Ribovski, R. Bron, I. S. Zuhorn, P. Rijn, *Chem. – A Eur. J.* **2020**, 26, 15084.
- [25] M. Tsintou, C. Wang, K. Dalamagkas, D. Weng, Y. N. Zhang, W. Niu, in *Nanobiomaterials Science, Development and Evaluation*, Elsevier Inc., Amsterdam **2017**, pp. 87–124.
- [26] M. A. Grimaudo, A. Concheiro, C. Alvarez-Lorenzo, *J. Control. Release* **2019**, 313, 148.
- [27] H. Wang, Q. Chen, S. Zhou, *Chem. Soc. Rev.* **2018**, 47, 4198.
- [28] G. Zu, M. Steinmüller, D. Keskin, H. C. Van der Mei, O. Mergel, P. Van Rijn, *ACS Appl. Polym. Mater.* **2020**, 2, 5779.
- [29] D. Keskin, O. Mergel, H. C. Van Der Mei, H. J. Busscher, P. Van Rijn, *Biomacromolecules* **2019**, 20, 243.
- [30] X. Wang, S. Yuan, D. Shi, Y. Yang, T. Jiang, S. Yan, H. Shi, S. Luan, J. Yin, *Appl. Surf. Sci.* **2016**, 375, 9.

- [31] G. Liu, K. Li, H. Wang, L. Ma, L. Yu, Y. Nie, *ACS Appl. Mater. Interfaces* **2020**, *12*, 16125.
- [32] A. W. Bridges, N. Singh, K. L. Burns, J. E. Babensee, L. Andrew Lyon, A. J. García, *Biomaterials* **2008**, *29*, 4605.
- [33] D. Mitra, E.-T. Kang, K. G. Neoh, *ACS Appl. Polym. Mater.* **2021**, *3*, 2233.
- [34] H. Yu, L. Liu, X. Li, R. Zhou, S. Yan, C. Li, S. Luan, J. Yin, H. Shi, *Chem. Eng. J.* **2019**, *360*, 1030.
- [35] C. Schlaich, M. Li, C. Cheng, I. S. Donskyi, L. Yu, G. Song, E. Osorio, Q. Wei, R. Haag, C. Schlaich, M. Li, C. Cheng, I. S. Donskyi, L. Yu, G. Song, E. Osorio, Q. Wei, R. Haag, *Adv. Mater. Interfaces* **2018**, *5*, 1701254.
- [36] Y. J. Fan, M. T. Pham, C. J. Huang, *Langmuir* **2019**, *35*, 1642.
- [37] L. Sigolaeva, D. Pergushov, M. Oelmann, S. Schwarz, M. Brugnoli, I. Kurochkin, F. Plamper, A. Fery, W. Richtering, *Polymers* **2018**, *10*, 791.
- [38] N. M. B. Smeets, T. Hoare, *J. Polym. Sci. Part A Polym. Chem.* **2013**, *51*, 3027.
- [39] X. Wu, R. H. Pelton, A. E. Hamielec, D. R. Woods, W. McPhee, *Colloid Polym. Sci.* **1994**, *272*, 467.
- [40] M. Andersson, S. L. Maunu, *J. Polym. Sci. Part B Polym. Phys.* **2006**, *44*, 3305.
- [41] F. A. Plamper, W. Richtering, *Acc. Chem. Res.* **2017**, *50*, 131.
- [42] B. Sierra-Martin, J. R. Retama, M. Laurenti, A. Fernández Barbero, E. López Cabarcos, *Adv. Colloid Interface Sci.* **2014**, *205*, 113.
- [43] Z. H. Farooqi, S. R. Khan, R. Begum, A. Ijaz, *Rev. Chem. Eng.* **2016**, *32*, 49.
- [44] O. Mergel, A. P. H. Gelissen, P. Wünnemann, A. Böker, U. Simon, F. A. Plamper, *J. Phys. Chem. C* **2014**, *118*, 26199.
- [45] N. Rabiee, S. Hajebi, M. Bagherzadeh, S. Ahmadi, M. Rabiee, H. Roghani-Mamaqani, M. Tahriri, L. Tayebi, M. R. Hamblin, *Acta Biomater.* **2019**, *92*, 1.
- [46] D. Keskin, L. Tromp, O. Mergel, G. Zu, E. Warszewik, H. C. Van der Mei, P. Van Rijn, *ACS Appl. Mater. Interfaces* **2020**, *12*, 57721.
- [47] M. T. Khorasani, H. Mirzadeh, *Radiat. Phys. Chem.* **2007**, *76*, 1011.
- [48] A. M. Trimukhe, K. N. Pandiyaraj, A. Tripathi, J. S. Melo, R. R. Deshmukh, in *Advanced Structured Material*, Springer Verlag, Berlin **2017**, pp. 95–166.
- [49] F. Walther, P. Davydovskaya, S. Zürcher, M. Kaiser, H. Herberg, A. M. Gigler, R. W. Stark, *J. Micromech. Microeng.* **2007**, *17*, 524.
- [50] M. Morra, E. Occhiello, F. Garbassi, *Surf. Interface Anal.* **1990**, *16*, 412.
- [51] O. Koniev, A. Wagner, *Chem. Soc. Rev.* **2015**, *44*, 5495.
- [52] L. K. Chaganti, N. Venkatakrishnan, K. Bose, *Biosci. Rep.* **2018**, *38*, BSR20181764.
- [53] H. M. F. Viart, T. S. Larsen, C. Tassone, T. L. Andresen, M. H. Clausen, *Chem. Commun.* **2014**, *50*, 7800.
- [54] S. Ramachandran, S. Thiyagarajan, G. Dhinakar Raj, A. Uma, *Int. J. Vet. Sci. Med.* **2017**, *5*, 187.
- [55] V. Audonnet, L. Malaquin, J. L. Viovy, *Bioanal. Rev.* **2011**, *3*, 41.
- [56] Z. H. Farooqi, H. U. Khan, S. M. Shah, M. Siddiq, *Arab. J. Chem.* **2017**, *10*, 329.
- [57] N. C. Martin, A. A. Pirie, L. V. Ford, C. L. Callaghan, K. McTurk, D. Lucy, D. G. Scrimger, *Sci. Justice - J. Forensic Sci. Soc.* **2006**, *46*, 179.
- [58] F. Tang, Y. Xie, H. Cao, H. Yang, X. Chen, J. Xiao, *Food Chem.* **2017**, *219*, 321.
- [59] F. Contu, B. Elsener, H. Böhnj, *J. Biomed. Mater. Res.* **2002**, *62*, 412.
- [60] J. Kim, M. Kim, S.-S. Nahm, D.-M. Lee, S. Pokharel, I. Choi, *Anim. Cells Syst.* **2011**, *15*, 147.
- [61] Z. Chen, R. Xu, Y. Zhang, N. Gu, *Nanoscale Res. Lett.* **2008**, *4*, 204.
- [62] H. T. M. Phan, S. Bartelt-Hunt, K. B. Rodenhausen, M. Schubert, J. C. Bartz, *PLoS One* **2015**, *10*, e0141282.
- [63] J.-C. Tseng, K. Vasquez, J. D. Peterson, Optical Imaging on the IVIS SpectrumCT System: General and Technical Considerations for 2D and 3D Imaging, **2015**, [https://www.perkinelmer.com/CMSResources/Images/44-171013TCH\\_012007\\_01\\_IVIS-2D\\_3D\\_Imaging.pdf](https://www.perkinelmer.com/CMSResources/Images/44-171013TCH_012007_01_IVIS-2D_3D_Imaging.pdf).
- [64] C. D. Klink, K. Junge, M. Binnebösel, H. P. Alizai, J. Otto, U. P. Neumann, U. Klinge, *J. Invest. Surg.* **2011**, *24*, 292.
- [65] B. D. Ratner, *J. Cardiovasc. Transl. Res.* **2011**, *4*, 523.
- [66] U. Klinge, B. Klosterhalfen, A. P. Öttinger, K. Junge, V. Schumpelick, *Biomaterials* **2002**, *23*, 3487.
- [67] J. M. Anderson, A. Rodriguez, D. T. Chang, *Semin. Immunol.* **2008**, *20*, 86.
- [68] L. Zhang, Z. Cao, T. Bai, L. Carr, J. R. Ella-Menye, C. Irvin, B. D. Ratner, S. Jiang, *Nat. Biotechnol.* **2013**, *31*, 553.
- [69] Z. Sheikh, P. J. Brooks, O. Barzilay, N. Fine, M. Glogauer, *Materials* **2015**, *8*, 5671.
- [70] H. Yan, C. Seignez, M. Hjorth, B. Winkeljann, M. Blakeley, O. Lieleg, M. Phillipson, T. Crouzier, H. Yan, M. Hjorth, M. Blakeley, T. Crouzier, C. Seignez, M. Phillipson, B. Winkeljann, O. Lieleg, *Adv. Funct. Mater.* **2019**, *29*, 1902581.
- [71] X. Xu, T. Jin, B. Zhang, H. Liu, Z. Ye, Q. Xu, H. Chen, B. Wang, *Polym. Test.* **2017**, *57*, 270.
- [72] Y. Qiao, Y. Li, Q. Zhang, Q. Wang, J. Gao, L. Wang, *Langmuir* **2020**, *36*, 5251.
- [73] S. Daghighi, J. Sjollema, A. Harapanahalli, R. J. B. Dijkstra, H. C. Van Der Mei, H. J. Busscher, *Int. J. Antimicrob. Agents* **2015**, *46*, 713.
- [74] P. P. M. Van Zuijlen, J. J. B. Ruarda, H. A. Van Veen, J. Van Marle, A. J. M. Van Trier, F. Groenevelt, R. W. Kreis, E. Middelkoop, *Burns* **2003**, *29*, 423.
- [75] D. Akilbekova, K. M. Bratlie, *PLoS One* **2015**, *10*, e0130386.
- [76] C. R. Morcombe, K. W. Zilm, *J. Magn. Reson.* **2003**, *162*, 479.
- [77] I. Scholz, P. Hodgkinson, B. H. Meier, M. Ernst, *J. Chem. Phys.* **2009**, *130*, 114510.
- [78] B. J. Van Rossum, H. Förster, H. J. M. De Groot, *J. Magn. Reson.* **1997**, *124*, 516.